DEMONSTRATION AT OOSTENDE

Written by Wikke Witteveen, Raf Meskens, Giani Ramos, Gerrit Van Geffen, Ruben Van Horebeke and Geert Potters – Antwerp Maritime Academy

The demonstrator

Location

Output 5 compares the conditions and corrosion rates of different port environments. We chose these locations to obtain a wide variety of different conditions:

- The south coast of England (Shoreham, Newhaven) which are in direct contact with the Atlantic Ocean.
- The port of Vlissingen, at the bank of the Westerschelde (leading directly into the North Sea).
- The port of Den Helder in the North of the Dutch province of Noord-Holland.
- The marina of Zelzate, along the canal of Ghent-Terneuzen, which is situated much more inland, and which offers brackish water.
- The port of Ostend, close to the North Sea.

Measurements in Ostend (part of Output 5 in the SOCORRO project) were performed on the dynamic platform DYPLA, built by the team at Antwerp Maritime Academy. This dynamic platform is located at ro-ro quay 202 in the Voorhaven of the port of Ostend at Slijkensesteenweg 4. It is situated at a few hundred meters of the port entrance, allowing access to real seawater and the inherent marine conditions, though there is a regular flow of less salty water past the platform, coming from the Spuikom (a local freshwater basin) or from inland waterways (through the Sas-Slijkens lock).

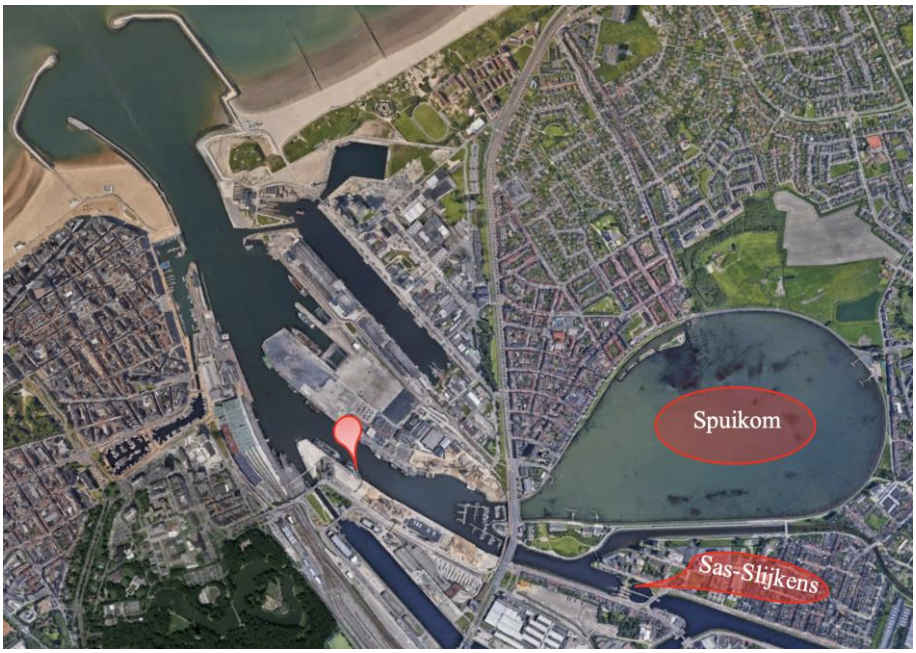

Figure 1. Location of the dynamic platform of Antwerp Maritime Academy.
Satellite image port of Ostend, with the position of the platform indicated with a red pin, and the Spuikom and the Sas-Slijkens lock indicated in red. Adapted from Google Earth

Figure 2. The dynamic platform at Quay RoRo202

Depth around the platform

The use of a floating pontoon as a platform ensured that both the racks and the sensors (see later) always remained submerged at a depth of 1 meter. In addition, the port of Ostend is characterized by an average tidal range of about 4 meters, resulting in significant tidal currents. These tidal currents are important in the context of corrosion research.

Depth soundings were taken in the wider area of the platform in 2016 by a sounding vessel (Figure 3). The location of the platform is indicated by the red rectangle in the centre right of the figure. Due to the size of the sounding vessel, it was impossible to sound under the bridges. Figure 4 shows 5 soundings taken on 27 November 2018 when the water level was 0 meters LAT. The bearing was taken under the loading bridge exactly at the position where the dynamic test platform is placed (red rectangle). This shows that the depth of the water at the location is approximately 2.30 meters.

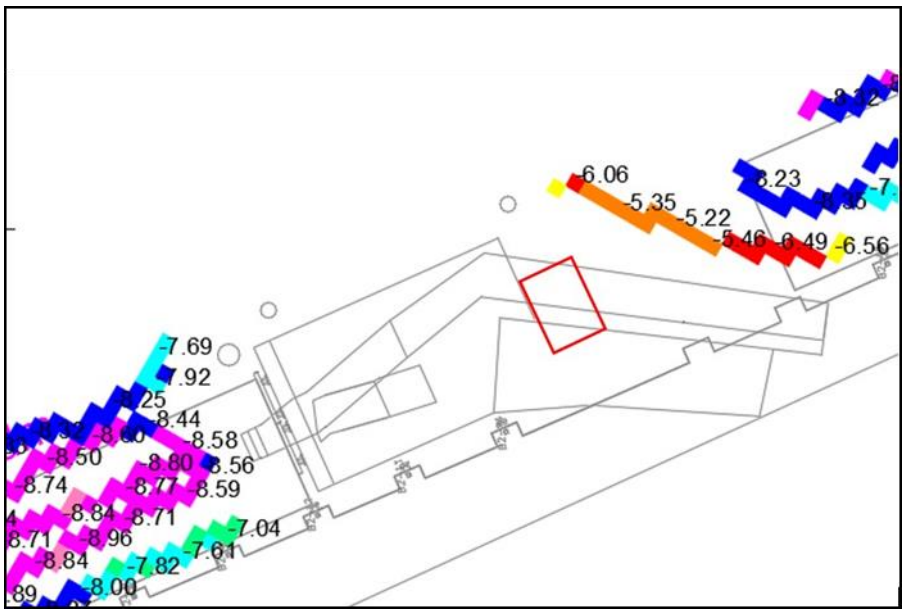

Figure 3. Depth sounding around the location of the DYPLA platform in 2016. Source: Port of Oostende (2016)

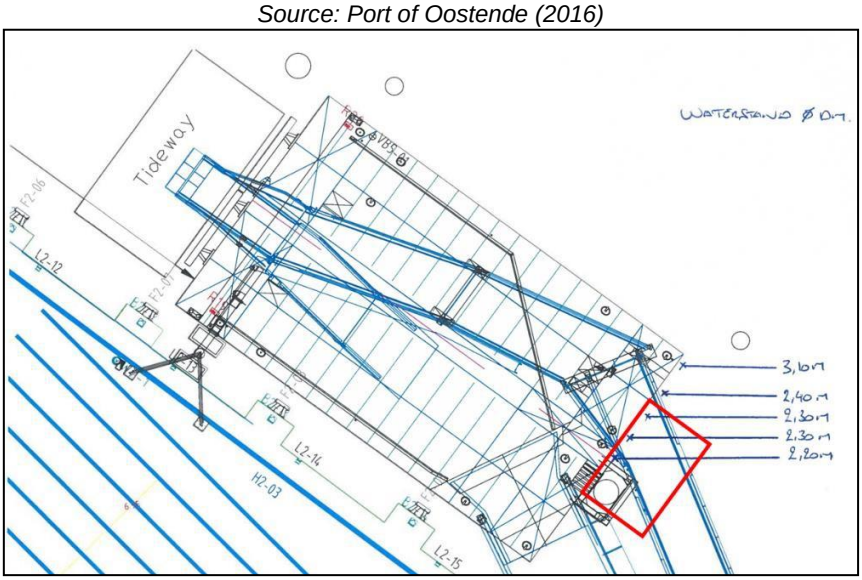

Figure 4. Depth sounding around the location of the DYPLA platform in 2018. Source: Port of Oostende (2018)

Sensor equipment

Both an environmental sensor (Scuba90) and a corrosion sensor (C-Cube) were used. By means of a specially designed distribution box, which was developed for the SOCORRO project, the uploading of data was optimized.

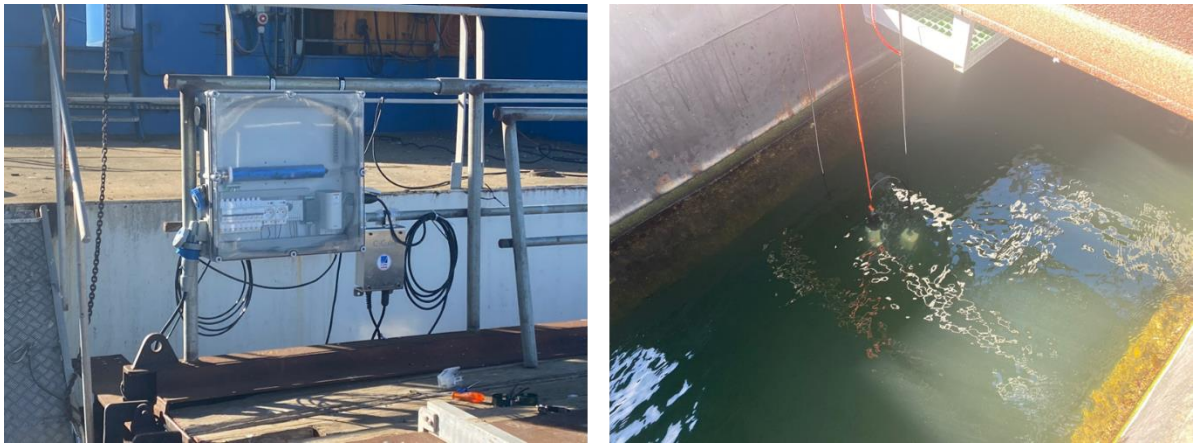

Figure 5. Sensor box installed on the DYPLA platform in Ostend.

A **Scuba90 sensor**, manufactured by Royal Eijkelkamp Soil & Water B.V., was used to measure the environmental parameters. (Giesbeek, The Netherlands). In the context of the SOCORRO project, only Scuba sensors were used, which measure specific environmental parameters that influence the corrosion rate. The measured physiochemical factors include temperature, pH, specific conductivity 25°C, salinity, dissolved oxygen, dry matter content, redox potential and chlorine content.

The Scuba90 sensor is 450mm in length and 90mm in diameter. The operating temperature varies within a range of -50°C to +50°C. The maximum operational depth of the sensor is 200 m, while the ion-selective electrode (ISE) can reach a maximum depth of 15 m. The sensor is supplied with a 12 V power supply and has a memory for 1,000,000 measurements (Royal Eijkelkamp, n.d.).

It is a multi-sensor probe equipped with several sensors capable of determining eight parameters (Royal Eijkelkamp, 2022).

- The **temperature** (Figure 6, 1) was measured by means of a thermistor whose resistance changes with temperature. Thermistors are very stable over time and therefore do not require calibration.
- **Dissolved oxygen** was measured using an optical sensor (Figure 6, 2). This sensor consists of a blue light source, a detection surface and a red-light receiver. When the detection surface is exposed to seawater, a reaction occurs between the oxygen in the seawater and the detection surface. The measurement principle is based on the phenomenon of fluorescence, where the detection surface absorbs light of a specific wavelength and then emits light of a different wavelength. In this case, the surface absorbs blue light and emits red light. During a measurement cycle, the blue light is turned on for a short time, after which the red-light receiver measures the time it takes for the fluorescence to extinguish. This length of time is proportional to the amount of dissolved oxygen in the seawater. It is important to emphasize that the presence of an oxygen active coating on the optical sensor can lead to inaccurate measurements. This is comparable to situations in which photosynthetic algae create a specific microenvironment of oxygen.

- The specific conductivity of water is determined by the four-electrode method. The sensor (Figure 6, 3) is equipped with two sets of graphite electrodes carefully positioned for stable measurement. A constant voltage is applied to one pair of electrodes and the current required to maintain this voltage is measured. The current strength increases as the conductivity of the water increases. The Scuba usually displayed specific conductivity, which is standardized to 25°C, representing the conductivity of the water as if the water had been heated or cooled to exactly 25°C. Conductivity can be expressed in different units, such as total dissolved solids (TDS) and salinity, expressed in Practical Salinity Unit (PSU). The values of either parameter were always derived from the specific conductivity.
- The acidity was determined by means of a pH glass electrode (Figure 6, 4). As a result of the ion exchange between the water and the pH glass membrane, a charge separation occurs across the glass. This charge separation creates a voltage difference that can be measured and corresponds to the pH value of the solution.
- The redox potential is measured using an oxidation-reduction potential (ORP) sensor (Figure 6, 5). This sensor is located next to the pH sensor and can be noticed as a gray dot of 1 mm diameter. The redox potential is determined by measuring the voltage drop between the platinum membrane of the ORP electrode and the reference electrode. Because platinum does not react with the ions in the water, the redox potential can be derived from this voltage drop.
- An extra fluorimeter (Figure 6, 6) can be used to measure the chlorophyll concentration in the water. This is a measure of the presence of microalgae and therefore an indicator of the biological activity of the marine ecosystem.
- A reference electrode (supporting the other electrode measurements; (Figure 6, 7) and a chloride sensor (Figure 6, 8) complete the setup.

The Scuba probe furthermore comes with two different attachments that serve to protect the sensors. These attachments can be securely attached to the sensors using threads. A sealed capsule is available to store the probe. Since the sensors must be stored in a humid environment, the sealed capsule is partially filled with water before being attached to the probe.

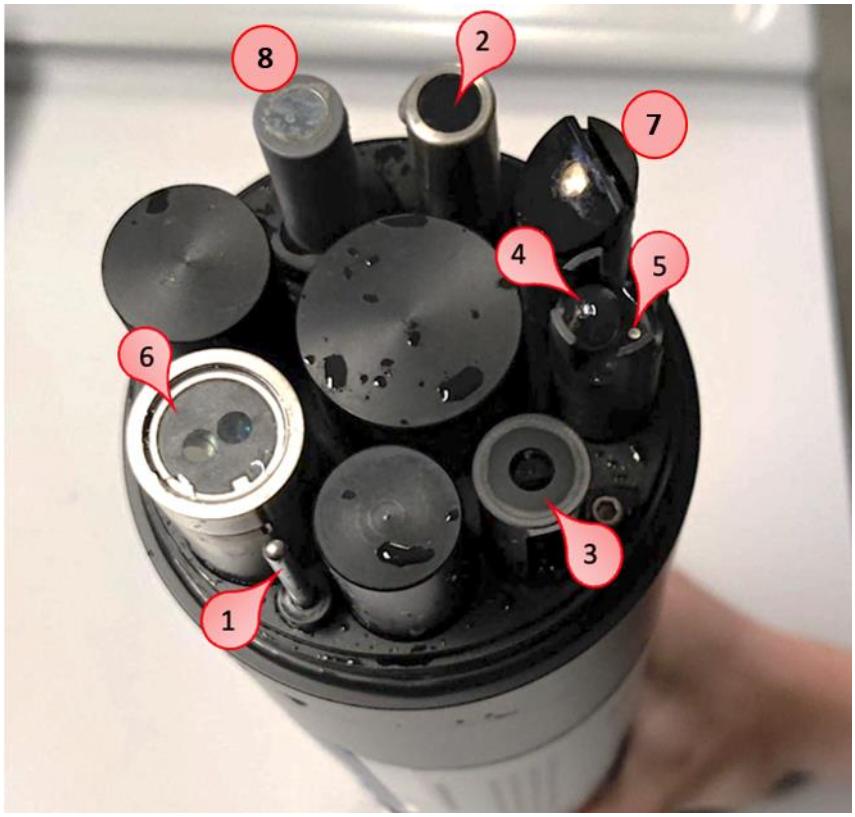

Figure 6. Different sensors of the Scuba Probe.
1: temperature sensor, 2: optical sensor (dissolved oxygen), 3: conductivity sensor, 4: pH glass, 5: ORP sensor, 6: fluorometer for chlorophyll determination; 7. reference electrode; 8. chloride sensor.

An open capsule (Figure 7) is used when the probe is deployed. This capsule contains a weight to sink the Scuba Probe. The openings in the capsule serve on the one hand for the efficient passage of water and on the other hand for the protection of the sensors.

Figure 7. Open capsule for a Scuba probe

The capsule is fitted with a copper mesh, which acts as a biofouling-resistant barrier. The copper mesh exhibits controlled solubility, slowly degrading and releasing copper ions. These copper ions cover the surfaces of the sensors and act effectively against the growth of biological organisms.

Scuba is connected to a 4G modem that uploads the data to the Telecontrolnet platform. Telecontrolnet is a platform where all data from the Scuba sensors come together. Here specific filters were applied to select only the sensors and parameters relevant for this project. Subsequently, a dataset was exported in the form of an Excel file. This Excel file was converted to a CSV file so that it was functional with the R program for the correlation analysis.

Calibration of the environmental sensors

When the secondary Scuba's readings differ from the in-water Scuba's readings, it was replaced or calibrated. The calibration procedure involves instructing the Scuba with the values it should indicate in a specific calibration situation, where the correct parameter value is known (Table 1). This practically implies the use of a liquid with a known value, which is indicated to the Scuba during immersion in this liquid.

Table 1. Calibration of the different sensors on the Scuba 90

Sensor	Calibration method	Calibration points
Temperature	No calibration needed	Not applicable
pH	Two-/three-points	pH 4, pH 7, pH 10
ORP	1 point	ORP standard 200 mV
Conductivity	1 point	CD standard, 0.5 M, 58670 µS (brackish – salt water) CD standard, 0.1 M, 12856 µS (brackish water) CD standard, 0.01 Molar, 1412 µS (freshwater) CD standard, 0.001 Molar, 147 µS (fresh/glacial water)
Dissolved oxygen	1 point	100% saturated distilled water (shaken heavily to saturate water with O_2)

Corrosion probes

For the SOCORRO project, a specific corrosion measurement system has been developed which measures corrosion of three different steel grades (S355, 316L and S235) and a micro-electrochemical cell that measures the rate of corrosion. These measurements are performed every 4 hours.

The linear polarisation (LP) sensor from CCube (Delft, the Netherlands) has dimensions of 150 mm (length) x 60 mm (height) x 50 mm (width). The working and reference electrodes are housed in a plastic housing filled with epoxy adhesive for protection against sea water.

The sensor is connected to a separate CCube control box located in an easily accessible position. A potentiostat and a data logger are installed in the control cabinet. In addition, the control box contains a mobile antenna that transmits the measured data to the CCube network. The company collects all sensor data and sends it to an online database that is accessible to all researchers of the SOCORRO project.

Sensor box

A sealed electrical distribution box was designed and built within the SOCORRO partnership to power the sensors and support the Scuba while uploading data. To this end, the distribution box is equipped with an internal heating element (Figure 8, 2) to maintain a constant temperature of approximately 15-20 degrees Celsius. This heating element is connected to a thermostat (Figure 8, 3) that controls the activation of the element when the temperature falls below the desired value and switches it off when the maximum temperature is reached. To prevent short circuits and electrical damage to the equipment, the entire distribution box is fitted with fuses (Figure 8, 4). In addition, two CEE 16A plugs (Figure 8, 5) are provided to connect a laptop or other electronic devices on site if necessary.

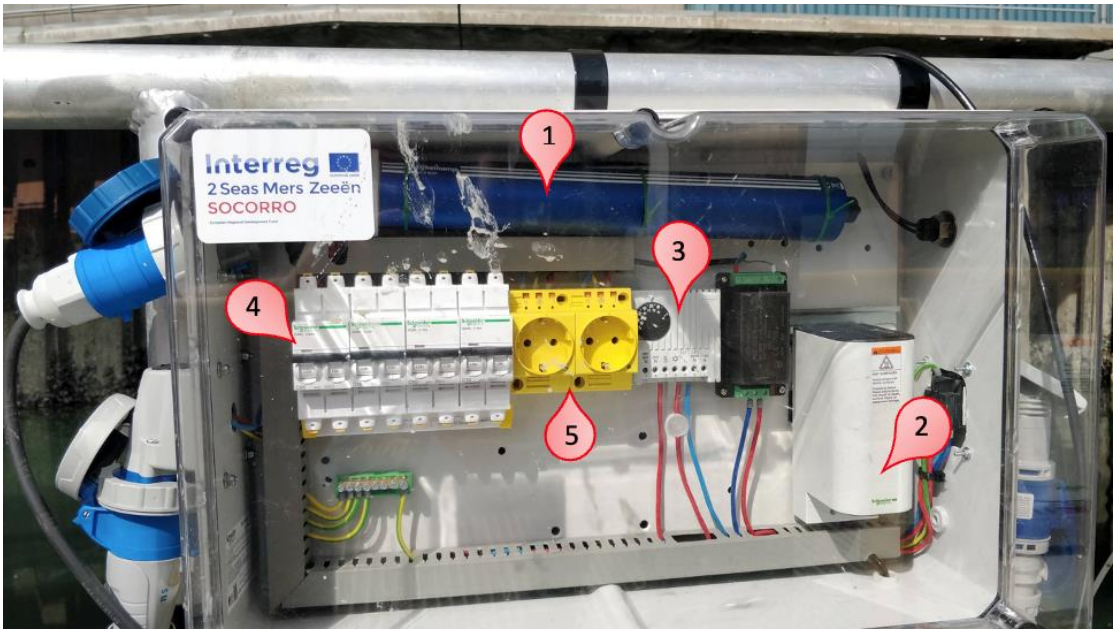

Figure 8. Electrical distribution box for sensors.
1: 4G modem, 2: internal heating, 3: thermostat, 4: circuit breakers, 5: sockets

Data upload

For this purpose, a 4G modem (Figure 8, 1), namely the GDT-S Prime Plus, is integrated in the system (Figure 46). This allowed the data generated by the Scuba sensors to be initially

stored and then forwarded to the GDT server at time intervals set by the user. Via this server, users not only had the possibility to view the data via the internet, but also to adjust the settings of the modem and sensors. This could be done via the Eijkelkamp web portal.

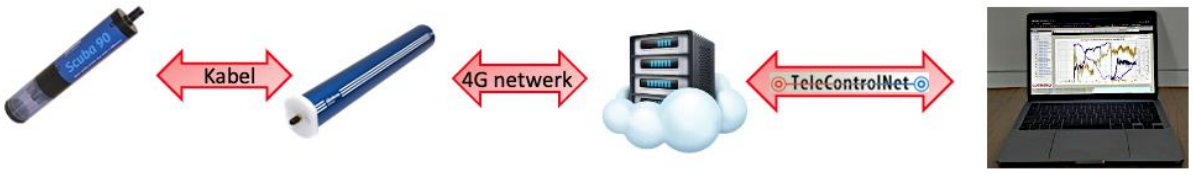

Figure 9. Overview of how data flows from sensor to web portal

Sensor maintenance

To ensure the accuracy of the measurements, it was essential to carry out a thorough maintenance of the sensors. At each visit to the rigs, the sensors were removed from the water and subjected to a thorough visual inspection. It was frequently found that the sensors suffered from biological fouling, which required careful and thorough cleaning. The cleaning process had to be carried out with extreme care to avoid possible damage to the sensors. It was crucial to clean specifically around the sensors and to avoid direct contact with the sensors. For the CCube corrosion probe, it was extremely important to have absolutely no contact with the LPR sensors, as this would disturb the corrosion layers already present on the sensor, which could affect the measurements.

For the maintenance of the Scuba, the initial concern is the external condition of the device. In particular, the copper protective cover, intended to limit biological growth on the sensors, may need to be replaced. Then the Scuba's current readings were analyzed using a secondary Scuba. A bucket was used to carefully collect a sample of water from the immediate vicinity of the setup, at a depth of about 1 meter. The bucket should be handled with care to minimize unwanted oxygen entry into the water. The Scuba was carefully placed in the bucket, to a distance of approximately 10 centimeters from the bottom, and then connected to a laptop computer running the Scuba Control Software. The direct measurement values could be observed via this software. After a certain period of time, the values stabilized. The software provided the option to copy a data series.

This data set was then compared to the data received from the Scubas in the water, allowing to calibrate or replace the Scuba to be determined. After the calibration procedure, the secondary Scuba was thoroughly rinsed with distilled water to remove any contaminants, and it was then safely stored, fitted with its protective cap, to maintain the integrity of the device.

Baseline measurements of environmental parameters

Two datasets can be used to describe the basic conditions at the platform in Ostend.

Short-term, diurnal data () come from a 24-hour long set of measurements taken on April 30, 2017, using Vernier lab probes, on water samples collected every hour. These data give us an overview of diurnal variation in the environmental conditions. To this end, temperature, oxygen content, turbidity, pH value, potential, salinity, nitrate concentration and chloride concentration of the seawater were measured every hour, at a depth of one meter and of five metres.

Long-term data with seasonal variation were collected between 3 August 2022 and 3 April 2023 at one meter depth, using the Eijkelkamp probes. Here, the data were collected every 30 minutes.

Diurnal measurements

The **seawater temperature** follows a comparable daily course for both a depth of 1 meter and a depth of 5 meters (Figure 10). Between four and five o'clock in the afternoon, a maximum is reached for both, 14.2 °C at a depth of 1 meter and 12.9 °C at a depth of 5 meters. Between five and six in the morning, the minimum temperature of 10.4 °C at a depth of 1 meter and 10.2 °C at a depth of 5 meters is reached.

The **dissolved oxygen concentration** (Figure 10C, D) shows a minimum around noon at both depths and a maximum between 4 and 7 am. These times for minima and maxima are the inverse of temperature. This can be explained by the fact that more oxygen can be dissolved in cold water. The standard errors of the measurement results at a depth of 1 and 5 meters are 0.159 mg/l and 0.121 mg/l respectively. This indicates that the measurements at a depth of 1 meter deviate more from the average value at that depth than the measurements at a depth of 5 meters. This can also be seen on the box plot.

Dissolved oxygen is a very important parameter to describe the ecological water quality. If there is a shortage of oxygen dissolved in the water, sensitive organisms will disappear. Too much oxygen is also not good, this can be harmful to the gills of fish. Oxygen enters the water through exchange at the water surface, but also through plants, algae and algae that carry out photosynthesis in the water. With eutrophication of the water, algal blooms may occur, which in turn can cause an excess of oxygen in the water (Vlaamse Mileumaatschappij, 2019; Lenntech, 2019).

Turbidity expressed in Nephelometric Turbidity Unit (NTU) is an arbitrary unit for the scattering of light passing through a liquid, caused by small particles that cannot be seen with the naked eye and are contained in the liquid. This phenomenon can be compared to smoke floating in the air. The NTU is a relative unit measured against a standard set by the United States Environmental Protection Agency (Wijnen, Anzalone, & Pearce, 2014). The mean turbidity value at 1 m depth was 41.70 NTU with a standard deviation of 11.96 NTU (Figure 10). At a depth of 5 meters, the value was 46.40 NTU with a standard deviation of 14.78 NTU.

The standard deviation at both depths is quite large. This means that the turbidity between different measurements differs a lot. The standard errors are 2.441 NTU and 3.019 NTU, respectively, indicating that the measurements are quite different from the mean.

Too high a turbidity can prevent sunlight from penetrating deep into the water. As a result, seaweeds and plankton are no longer or insufficiently able to photosynthesise, causing them to die (Stevenson, Piper, & Confer, 1979).

The average **pH value** at a depth of 1 meter was 8.26 with a standard deviation of 0.08 (Figure 10). At a depth of 5 meters, the pH value is 8.33 with a standard deviation of 0.07. From this it can be concluded that the measurements of the pH values are very close to each other. The standard error at 1 and 5 meters is 0.016 and 0.014 respectively. A pH of about 8.2 is considered normal for seawater (Hall-Spencer et al., 2008).

The average concentration of nitrates at a depth of 1 meter was 49.7 ± 1.5 mg/l. At a depth of 5 meters this concentration was 67.0 ± 1.6 mg/l (Figure 11, A&B). The European Community has set a maximum concentration of 50 mg/l for nitrates. This is to protect public health and prevent eutrophication (Flemish Environment Agency, 2017; European Council, 1991). On average, this maximum value was just not exceeded at a depth of 1 metre. If the individual measurements are considered, it was exceeded several times. At a depth of 5 metres, the average does exceed this maximum value. Not all coastal ecosystems respond to eutrophication in the same way. Different characteristics of the ecosystem will determine the response of the coastal waters to an increase in nutrients. These can be both physical (tidal dynamics, residence time, turbidity, depth) and biological characteristics (presence of benthos) (Cloern, 2001). An example of this different response is the difference between the river Scheldt and the estuary of this river, namely the Western Scheldt. As a result of eutrophication, a large algae bloom occurs on the river Scheldt. Not on the Western Scheldt, on the other hand. The algal bloom is hindered by the high turbidity and mixing of the water (Kromkamp, Peene, van Rijswijk, Sandee, & Goosen, 1995; Prins, Bot, Duin, & Peeters, 2002).

When interpreting the measurement results of the nitrate sensor, it must be taken into account that chloride ions have a disturbing effect on this sensor (Vernier, 2018). The measurements were carried out in seawater, which logically contains many chloride ions.

Salinity is the total of all salts that are not carbonates dissolved in water. Salinity is expressed in parts per thousand or promille (Vernier, 2014). The average salinity at a depth of one meter was 19.01 ‰ and at a depth of five meters 27.86 ‰ (Figure 11, C&D). This difference is due to fresh water from, for example, rain that mixes with seawater and thus reduces the concentration of salt in the upper layer of water. There is also a supply of fresh water from the Ghent-Bruges-Ostend canal. At a depth of 1 meter, a similarity can be seen with the semi-diurnal tide of the Belgian coast. Semi-diurnal means that there are high tides twice a day and low tides twice a day. On April 29, the high tide was at 4:05 PM and on April 30 at 4:27 AM. Around these times, salinity reached a maximum value. It was low tide at 22:51 on April 29 and at 11:16 on April 30. Around these times, salinity reached a minimum value.

There are different scales to classify water according to salinity. What most of these scales get right is that they speak of salt water from 30 ‰ (Dahl, 1956; Ekman & Palmer, 1953;

Remane, 1934; Välikangas, 1933). The average salinity of the oceans is between 30‰ and 50‰ (Dahl, 1956). The disc will therefore rotate in brackish water.

Seawater has a fairly constant concentration of **chloride ions**. This was also evident in the measurements shown by graphs G1 and G2. At a depth of 1 meter the average concentration was 12.78 mg/l and at a depth of 5 meters it was 19.88 mg/l. The difference between the depths may be due to the supply of fresh water from the Ostend-Bruges canal.

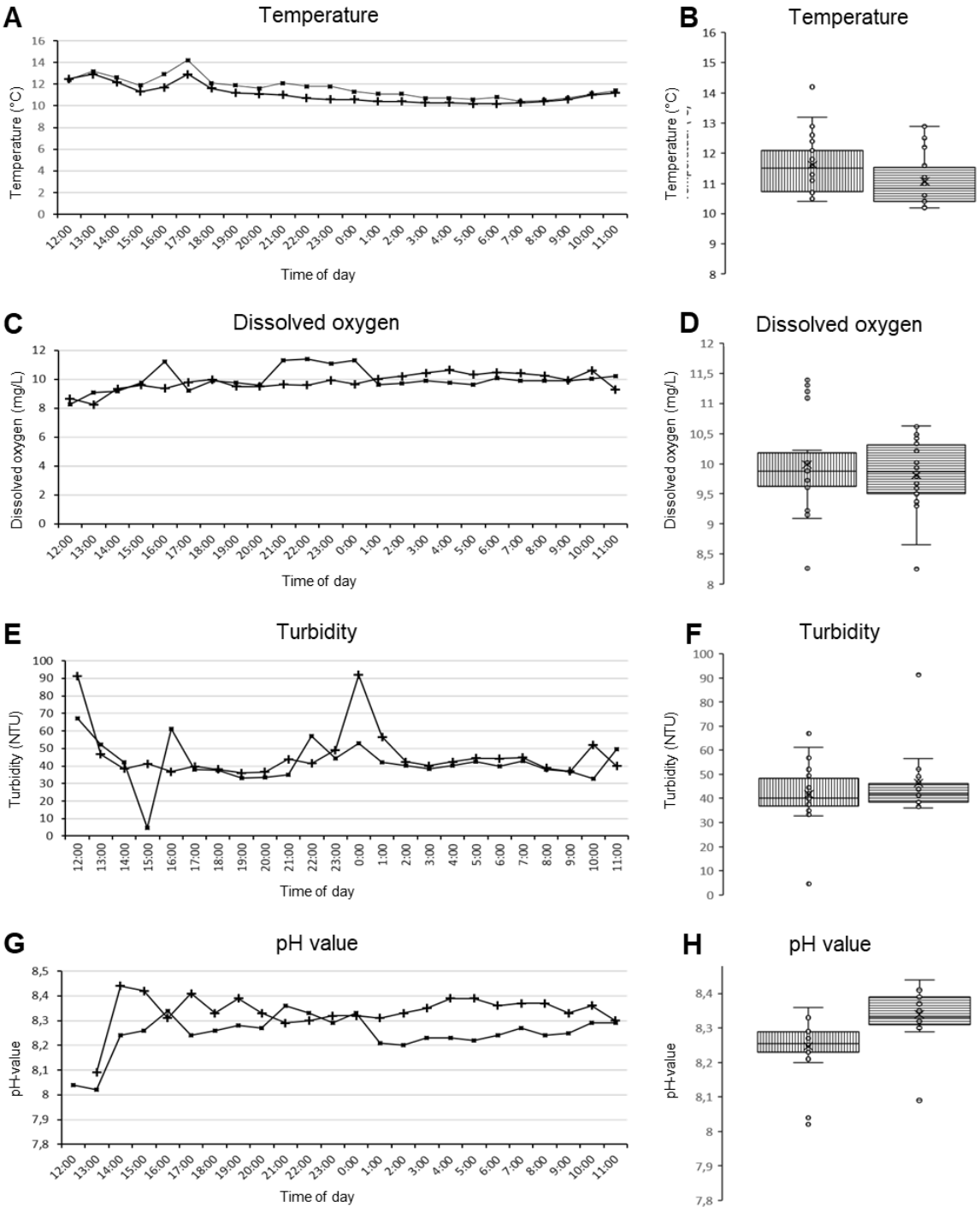

Figure 10. Diurnal patterns in physicochemical characteristics of water samples at the Ostend measuring site. (A) Time kinetics and (B) distribution of seawater temperature; (C) time kinetics and (D) distribution of the concentration of dissolved oxygen; (E) time kinetics and (F) distribution of turbidity values; (G) time kinetics and (H) distribution of pH values. ■: measurement at 1 m depth. +: measurement at 5 m depth. For the boxplots: left: 1 m depth, right: 5 m depth.

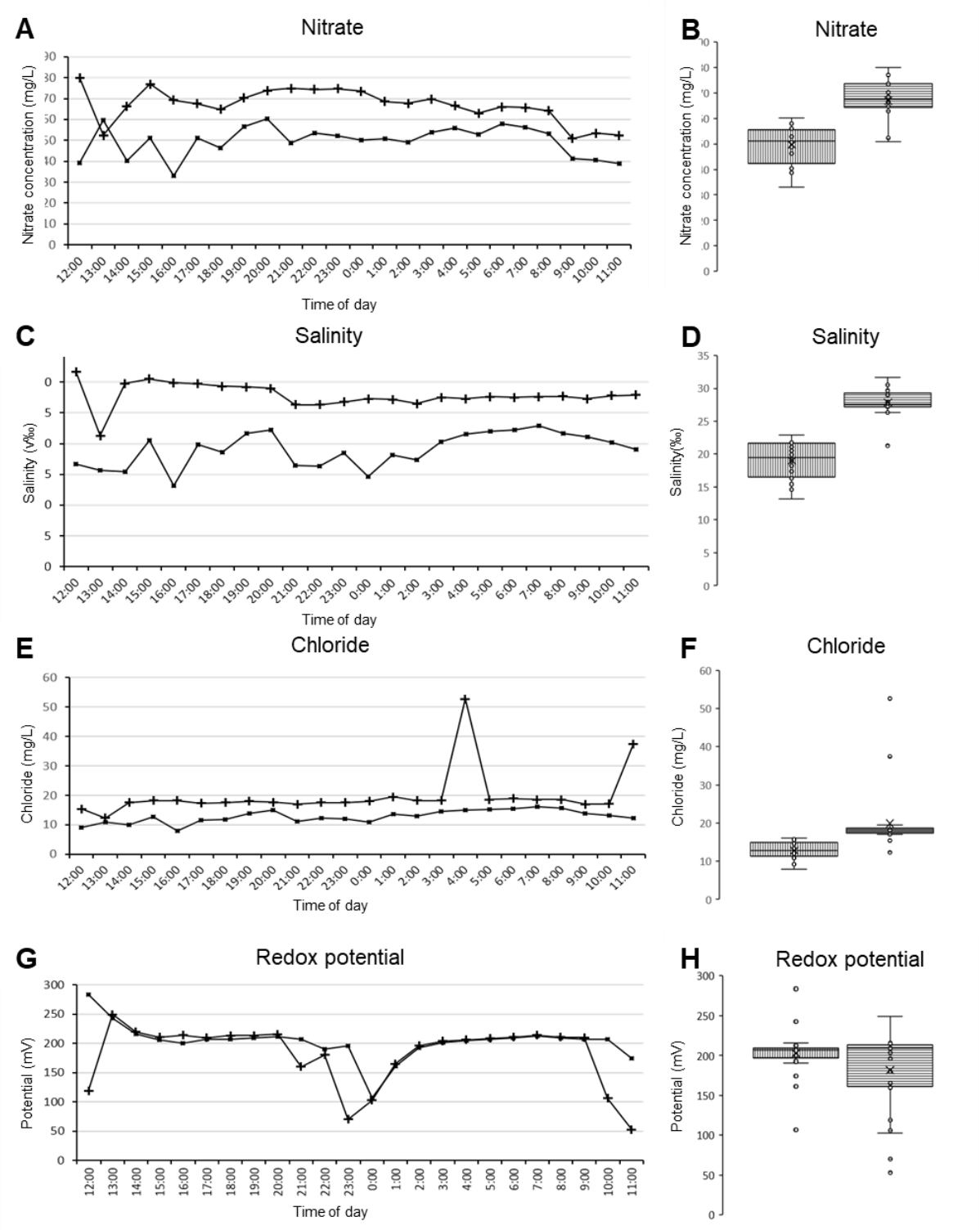
A
Nitrate
Nitrate concentration (mg/L)
Time of day
B
Nitrate
Nitrate concentration (mg/L)
C
Salinity
Salinity (‰)
Time of day
D
Salinity
Salinity(‰)
E
Chloride
Chloride (mg/L)
Time of day
F
Chloride
Chloride (mg/L)
G
Redox potential
Potential (mV)
Time of day
H
Redox potential
Potential (mV)

Figure 11. Diurnal patterns in physicochemical characteristics of water samples at the Ostend measuring site. (A) Time kinetics and (B) distribution of nitrate content values; (C) time kinetics and (D) distribution of the salinity; (E) time kinetics and (F) distribution of chloride concentration values; (G) time kinetics and (H) distribution of the redox potential of the water. ■: measurement at 1 m depth. +: measurement at 5 m depth. For the boxplots: left: 1 m depth, right: 5 m depth.

Seasonal measurements

Between August and September, the **temperature** varies between 21°C and 23°C, with a peak of 24°C (Figure 12, left). From September onwards, the temperature starts to drop gradually, with an abrupt drop from 20°C to 15°C in the middle of the month, followed by a slight rise to 17°C. At the end of September, the temperature stabilizes at 15°C. From October to November the temperature remains constant at 15°C. The temperature then drops linearly from 15°C to the minimum observed level of 1°C in December. Thereafter, there is an increase of 1°C to 10°C from mid-December to early January. Then a turning point is observed, where the temperature begins to decrease again. The box plot clearly shows that 50% of the observations are above 15°C and the other 50% are below 15°C (Figure 12, rght). This distribution is fairly symmetrical.

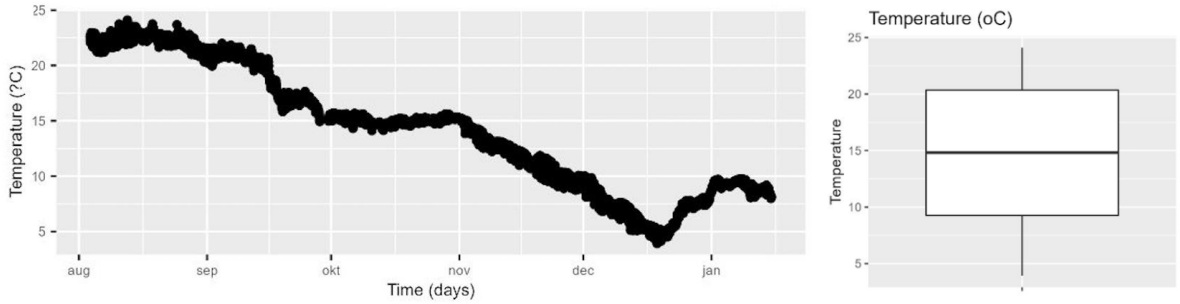

Figure 12. Temperature development of the water in the port of Ostend as a function of time (left) and represented in a boxplot (right).

In the initial stage of the measurement, until September, the **dissolved oxygen content** shows significant variation between 3 mg/L and 6 mg/L without a clear pattern (Figure 13). Subsequently, there is a decrease to 2 mg/L in mid-September. Thereafter a significant increase is observed to about 6 mg/L. From this point, the dissolved oxygen level stabilizes between 4 and 6 mg/L until the end of October. At the beginning of November, the dissolved oxygen content rises to a maximum of 9 mg/L in mid-December. Thereafter there is a slight decrease until the beginning of January, followed by a further increase. There is clearly an inverse relationship to the time series of temperature (Figure 13). The boxplot indicates an average of 6.25 mg/L over the whole period, with a symmetrical distribution.

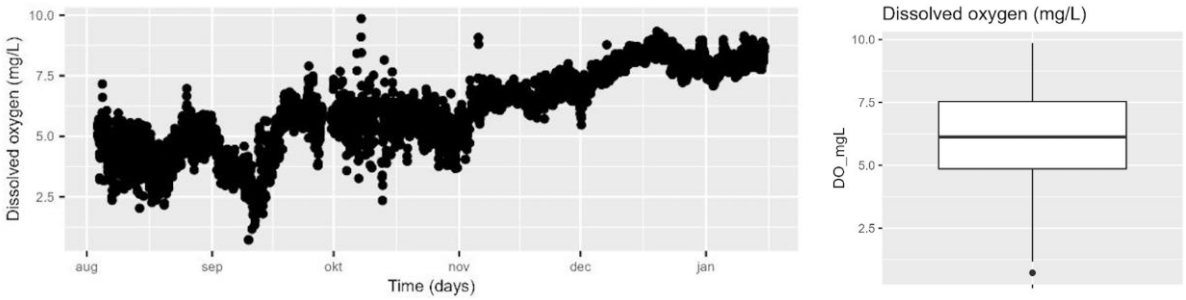

Figure 13. Dissolved oxygen in the water in the port of Ostend as a function of time (left) and represented in a boxplot (right).

Salinity (Figure 14) and **specific conductivity (standardized at 25°C)** (Figure 15) remain relatively stable from the beginning of August to the first week of September, with an average value of about 30 PSU (or 45 mS/cm). with a notable anomaly in mid-August, where the conductivity briefly dropped to 12 PSU (20 mS/cm). From the first week of September, no clearly recognizable pattern can be discerned due to the considerable variations. The conductivity varies during this period between a maximum of 50 mS/cm and a minimum of approximately 5 mS/cm or a salinity between a maximum of 33 PSU and a minimum of about 2 PSU.

For 50% of the measurements are above 37 mS/cm (24 PSU) and the other 50% are below 37 mS/cm. It is remarkable that there is more variation in the values below 37 mS/cm than in the values above 37 mS/cm, as indicated by the skewness of the distribution. This can be explained by the fact that the values from August to the first week of September were stable above 40 mS/cm, resulting in less variation in the values above 37 mS/cm.

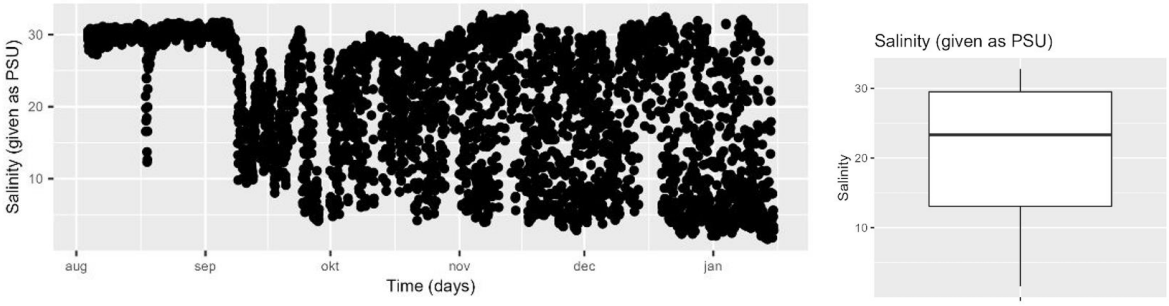

Figure 14. Salinity of the water in the port of Ostend as a function of time (left) and represented in a boxplot (right).

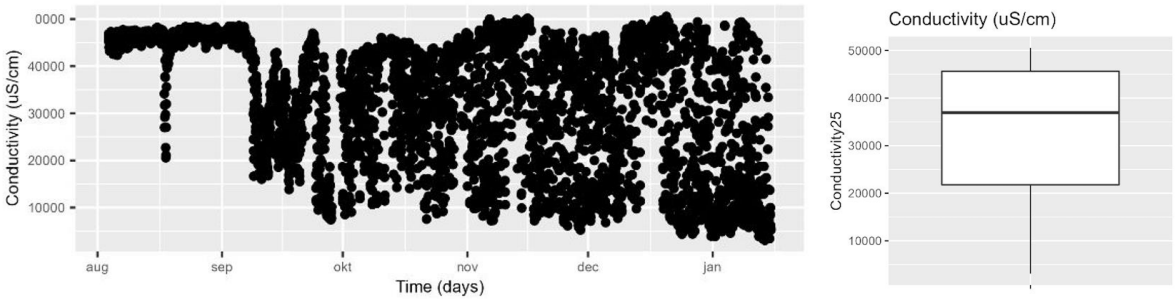

Figure 15. Conductivity (standardised at 25°C) of the water in the port of Ostend as a function of time (left) and represented in a boxplot (right).

These fluctuations can be explained by looking at possible influences from the inland water flowing through the Port of Ostend. Theoretically, it could be argued that the presence of the Spuikom (a sluice basin in the port of Ostend) can have various consequences on the corrosion behaviour of the coupons. The salt concentration in the basin varies depending on the degree of mixing between the drain water from the port and the surrounding water. When the sluice gates are opened, the water flows from the port to the Spuikom, causing a mixing of the salty harbour water and the water in the sluice basin. However, further investigation revealed that the influence of the Spuikom on the measurements was negligible, the connection between the port of Ostend and the Spuikom itself is a drainage system, and not a sluice basin. Moreover, the exchanges of water between the Spuikom and the port are very minimal and involve an exchange from salt water to salt water. It should also be noted that the gates of the drainage construction are not completely watertight, so that there is always a continuous exchange of water between the port and the Spuikom. On the other hand, the Sas-Slijkens lock turned out to be a substantial factor in the interpretation of the measurements. Fresh water comes from the Ghent-Bruges-Ostend Canal and is injected daily for several hours into the port of Ostend through openings in the lock gates. This equates to a flow rate of 30-40 m^3 of fresh water per second, which had had an influence on the measurement results. In the July-August 2022 dry period, water was injected once in August, as can be seen in the data. This variation in salinity could result in a reduced salt concentration in the port. At higher evaporation rates, the salt concentration in the water increases, while the supply of fresh water reduces the salt concentration. The Spuikom or the water passing through the lock could also influence the flow patterns and turbulence in the port of Ostend. This can lead to increased mechanical loads on the coupons, which can lead to erosion corrosion. In addition, changes in flow patterns can also affect the local concentration of corrosive elements or lead to the transport of contaminants and particles, such as sediments, rust particles and biological organisms. These particles can adhere to metal surfaces and accelerate corrosion processes by creating locally corrosive environments or causing mechanical damage.

The **pH values** in Ostend are evenly distributed around a central tendency of pH 8 (Figure 16). Almost all observations are within a range of 7.75 to 8.25, with only a few outliers. This suggests that the pH of the water in Ostend is mainly basic and that most values are close to a pH of 8 during the measurement period.

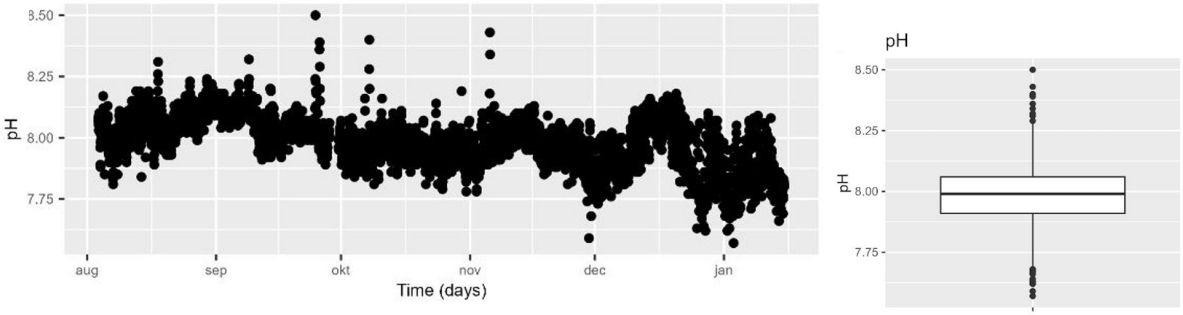

Figure 16. pH of the water in the port of Ostend as a function of time (left) and represented in a boxplot (right).

The observed **redox potential** (oxidation-reduction potential, ORP) in the first half of August, shows a pattern of a significant increase from the initial value from 100 mV to 250 mV, followed by a downward trend to 150 mV (Figure 17). From this point until the beginning of October, the redox potential shows a linear increase to 500 mV, with some peaks in the first half of September. During the period from the beginning of October to the beginning of November, a downward trend is observed, with the redox potential falling by 50 mV to a value of 450 mV. From this point until mid-January, the redox potential remains constant at around 450 mV. The distribution of the ORP values is symmetrical around the median, which is at 450 mV. It is striking that there is much less spread for values above 450 mV than for values below 450 mV. This can be attributed to the stabilization of the redox potential between the values of 400 and 500 mV from October.

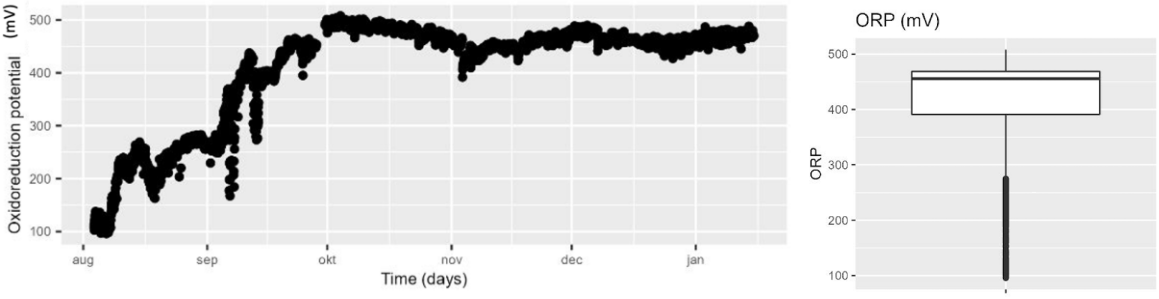

Figure 17. Oxido-reduction potential of the water in the port of Ostend as a function of time (left) and represented in a boxplot (right).

Correlations between environmental parameters

For the discussion of the correlation of the parameters, this study is limited to the relationships with an absolute correlation coefficient above 0.700, which corresponds to a high correlation (Figure 18). Of course, this coefficient must also be critically compared with the distribution in the scatter plot. For example, a high correlation coefficient may have been obtained with a scatter plot that is clearly difficult to interpret.

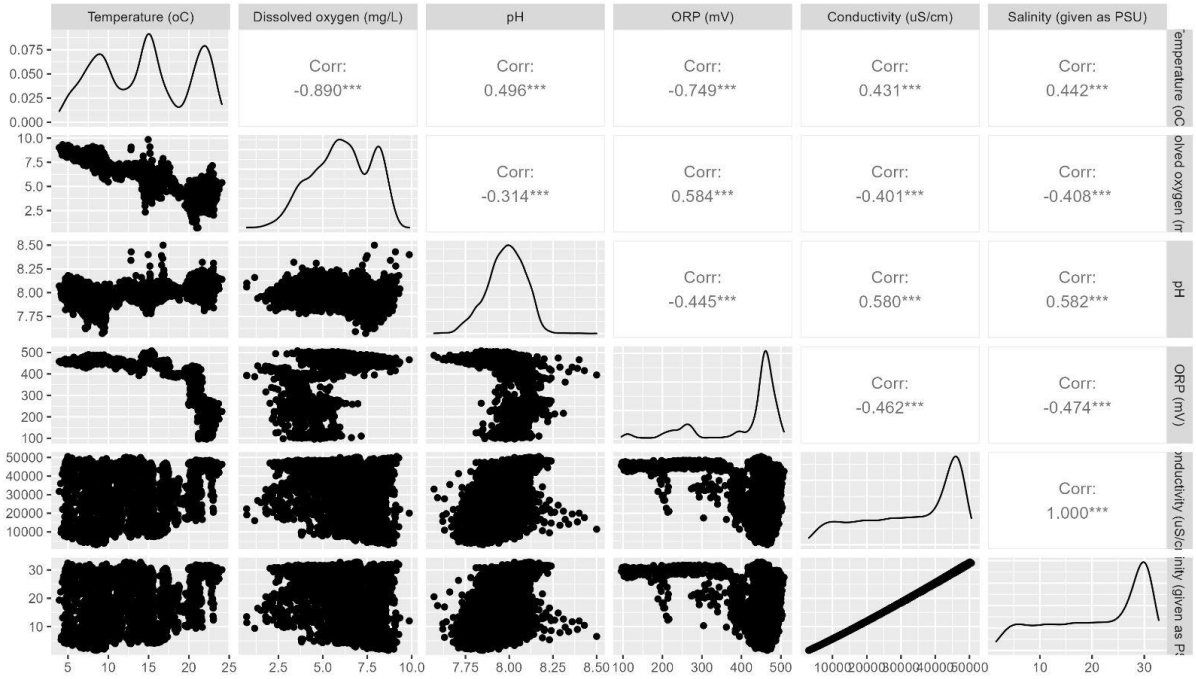

Figure 18. Correlation between the different environmental parameters in Ostend

With a correlation coefficient of -0.890 and an associated favorable dot plot, it is concluded that there is an inverse relationship between temperature and dissolved oxygen (Figure 18). The fact that the temperature of the water mass is one of the main factors influencing the dissolved oxygen content is also confirmed in the literature (Ma et al., 2021). In general, warm water has a reduced ability to hold oxygen, while cold water can hold more oxygen. At higher water temperatures, water molecules have more energy, making them less able to retain oxygen molecules. This results in a lower solubility of oxygen in the water. At lower water temperatures, the water is able to hold more oxygen molecules. This is because water molecules have less energy at lower temperatures and are therefore better able to absorb oxygen molecules. This is clearly visible upon comparison of the time series (Figure 12) and the dissolved oxygen graphs (Figure 13) where the dissolved oxygen content increases as the temperature of the water decreases. Indeed, the corrosion rate of steel in water is approximately proportional to the oxygen concentration up to 10 mg/L. At higher concentrations, the corrosion rate decreases sharply. This is due to the fact that the gas permeates more easily the $Fe(OH)_2$ layer which initially forms at lower concentrations of oxygen than the $Fe(OH)_3$ layer which forms at higher oxygen concentrations. This $Fe(OH)_3$ will also precipitate on the metal as a passivation layer.

The solubility of oxygen is also inversely proportional to temperature. The equation of Tromans (1997) shows the effect of the partial pressure of oxygen (P_{O2}) in the atmosphere and temperature (T) in Kelvin, on the molar concentration of dissolved oxygen(c_{aq}):

$$c_{aq} = P_{O_2}\left\{\frac{0{,}046T^2 + 203{,}357T\ln\left(T/298\right) - (299{,}378 + 0{,}092T)(T - 298) - 20{,}591 \times 10^3}{(8{,}3144)T}\right\}$$

At normal temperatures, the presence of dissolved oxygen is necessary to observe noticeable corrosion phenomena. In the absence of dissolved oxygen at room temperature, the corrosion rate of iron and steel is negligible. When oxygen and temperature vary together, the effect of oxygen predominates.

Although a plausible relationship can be seen between the temperature and the redox potential, the scatterplot is not linear here. This is confirmed by a correlation coefficient of -0.749. For example, changes in temperature can affect the rate of chemical reactions in the water, which in turn can affect the redox reactions. Higher temperatures generally speed up chemical reactions, while lower temperatures slow down the reaction rate. These changes in reaction rate can eventually lead to changes in the redox potential of the seawater. This is also confirmed in the literature (Ma et al., 2021).

Since the fluctuations in pH values remain virtually unchanged over the entire measurement period, it can be concluded that pH is not influenced by the other environmental factors (Figure 18). The relatively high correlation coefficients obtained are due to the use of a very small scale for the pH value.

As salinity is derived directly from the specific conductivity, Figure 18 shows a directly proportional relationship, as indicated by the correlation coefficient of 1.00.

Principal component analysis

The first principal component already explains 63% of the total variance of the dataset, while the second principal component explains 20% of the total variance of the dataset. In this way, 83% of the total variance can be described in a two-dimensional PCA plot (Figure 19).

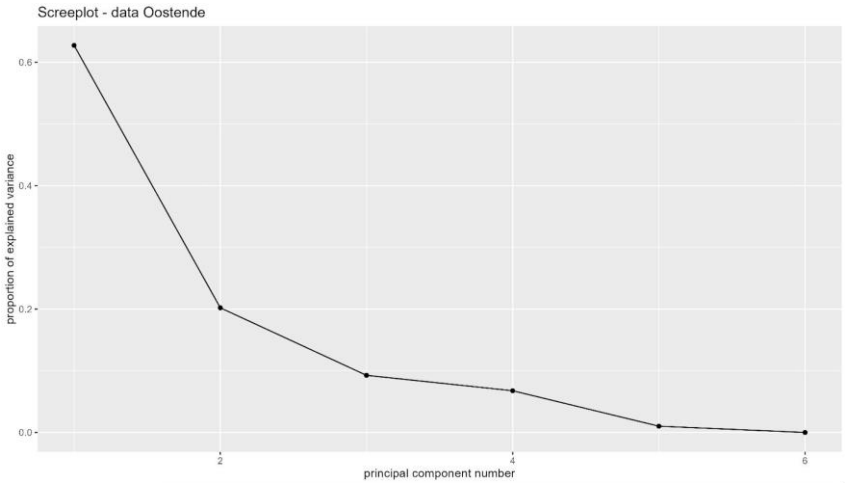

Figure 19. Scree plot for the PCA analysis of the environmental parameters at the Ostend demonstrator

The PCA confirms the inverse relationship between temperature and dissolved oxygen (Figure 20). Also, the dissolved oxygen content and the redox potential are positively correlated, while they are negatively correlated with temperature. However, the relationship between the redox potential and the other variables, such as dissolved oxygen and temperature, is more complex than a simple linear relationship. In reality, there is no direct proportional relationship between redox potential and dissolved oxygen, nor an inverse relationship with temperature. This is also confirmed by the dot plot (Figure 62), which shows that there is no clear linear relationship between these variables. In addition, the PCA shows that the specific conductivity and salinity are almost perfectly proportional. This is because salinity is calculated directly from the conductivity.

As for pH, the PCA shows that there is no relationship between pH and the group of temperature, redox potential and dissolved oxygen. Although the PCA plot suggests that there is a proportional relationship between pH and salinity on the one hand and specific conductivity on the other, the correlation analysis shows that this is not the case. It is suspected in this study that the data may have been over-magnified in the PCA analysis, creating relationships that are not actually present.

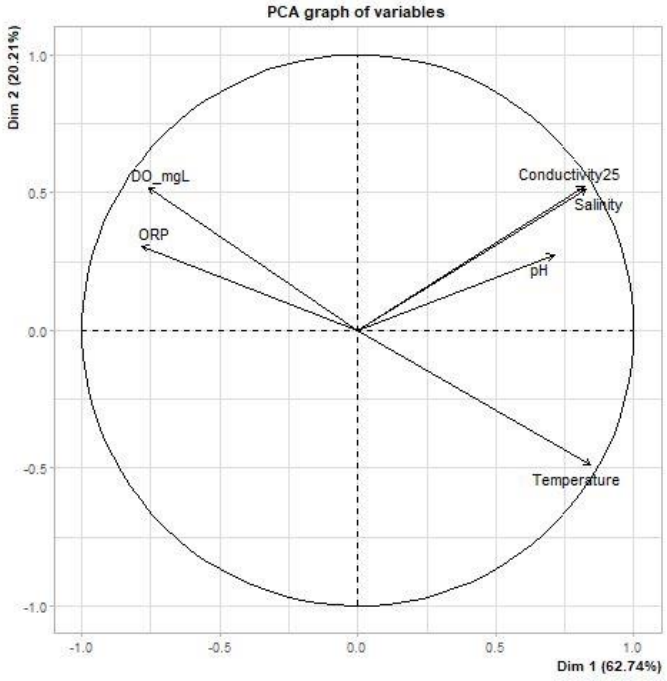

Figure 20. PCA biplot for the environmental data of the Ostend demonstrator

Organisms to be expected in the water

From previous experiments, carried out between December 13, 2017 and September 26, 2018, in which coated and bare steel plates were exposed to the dock water in the port of Ostend for 287 days, we know that the following organisms will settle on any material present in the water: mussels, sea squirts, barnacles, sponges, worm tubes, oysters and seaweed. In addition to these macro-organisms, a biofilm has most likely also formed. It was therefore

deemed necessary to equip the long-term sensors (Royal Eijkelkamp) with a copper mesh to avoid fouling, and later even with a sensor brush, to remove settling larvae from the sensor heads.

Corrosion measurements: experimental methodology

Steel types

Three specific steel types were selected for conducting the experiments: S235, S355 and 316L. In the following paragraphs, these individual steel types will be briefly described, explaining their characteristics and composition.

The first material is **S355 carbon steel**, which meets the European EN 10025:2 standard. This is a structural steel type (indicated by the "S" in the designation, which refers to "structural"). The value "355" stands for the minimum tensile strength of the material (355 MPa, for a sheet thickness of 16 mm). S355 can be classified as "mild steel" because of its relatively low carbon content, which makes it more suitable for welding work (de Jesus et al., 2012). The chemical and mechanical properties of the steel can be compared to those of the American standard variant ASTM A572/A709 (Igwemezie, Mehmanparast, & Kolios, 2018). S355 is widely used in various construction applications, including shipbuilding, bridge components, offshore structures and wind towers (Igwemezie et al., 2018).

S235 carbon steel follows the guidelines of the European Committee for Iron and Steel Standardization (ECISS), with a minimum tensile strength that is slightly lower than that of S355 for an equal thickness.

Both aforementioned structural steels belong to the category of low-carbon steels. The carbon limit for this category has been set at 0.30%, with both S235 with a maximum value of 0.22% C and S355 with a maximum value of 0.23% C more than comply. In addition to the carbon content, the American Iron and Steel Institute (AISI) also looks at the alloying elements in the steel. Since both S235 and S355 have a manganese content of up to 1.60%, they are classified as "plain carbon steel" (Singh, 2020). These classifications and limit values provide insight into the composition and properties of the steels. It is important to note that these low carbon steels will not perform optimally in terms of corrosion resistance. The material does not contain the crucial elements such as copper, chromium or nickel, which are of great importance for corrosion resistance. In the past, this material was available in a pickled and oiled form, which offered some degree of corrosion resistance.

Alloy 316L is a stainless steel with an austenitic structure containing chromium, nickel and molybdenum. The molybdenum improves corrosion resistance and resistance to pitting corrosion caused by chloride ion solutions, which often occur in water. In addition, it also increases strength at high temperatures. To provide protection against corrosion, a thin layer of metal oxides is applied to the surface, which acts as a barrier against corrosive substances. Typically, alloy 316L contains approximately 2-3% molybdenum, 16-18% chromium, 10%-14% nickel, 16-18% chromium, and 0.08% carbon. Other elements can be added to this alloy to modify the properties of the steel. Alloy 316L is widely used in marine equipment, refineries and chemical plants because of its excellent corrosion resistance, especially in highly corrosive environments.

Use of coupons for corrosion measurements

To completely submerge the metal coupons in water, racks were used to which the coupons were attached. To enable this attachment, two 8 mm diameter holes were drilled into the coupons. These holes were then used to securely fasten the coupons to the rack using tie wraps. Color coded tags were used to ensure that the different coupons could be identified throughout the study. These tags were attached individually to each plate, as well as to the rack itself. This made it possible to keep an overview of which coupons were still in the water and which had already been removed from the water. These identification tags were essential to enable proper tracking and analysis of the coupons throughout the research process.

The racks themselves were constructed using cut wire panels (Figure 21). This created a rectangular rack consisting of a grid of 3 by 9 compartments, resulting in a total of 27 coupons that could be attached to the rack. The racks themselves were also tagged, which were linked to specific locations. These tags were of a different color so that locations where the racks were used could be identified later. This tagging method was instrumental in maintaining traceability and facilitating the accurate identification of both coupons and racks throughout the research process.

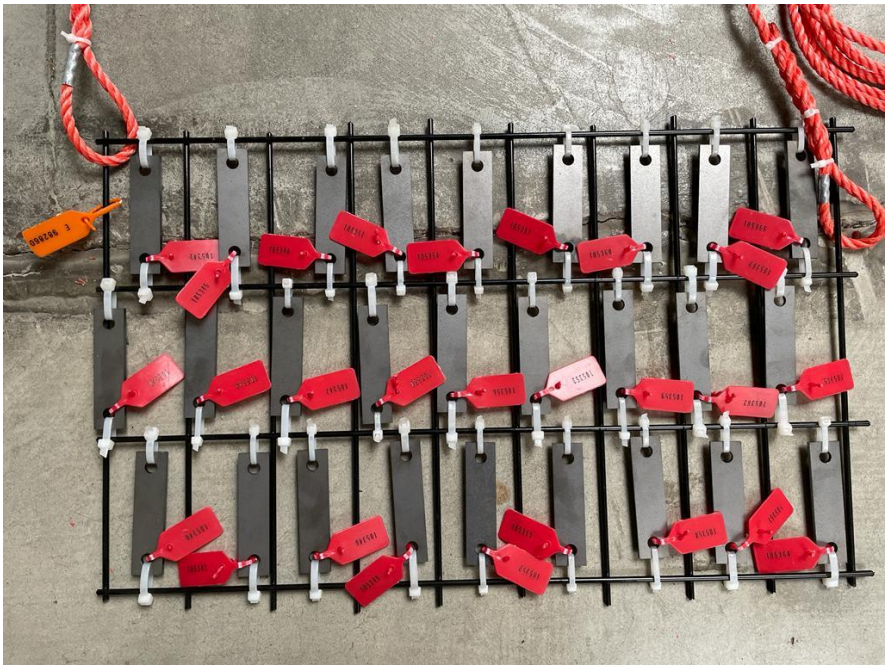

Figure 21. Rack of S355 coupons to be exposed to the seawater in Ostend

The racks were attached by means of an eye splice made of three-strand twisted polypropylene rope, whereby the corners of the rack were attached to this rope. To keep the rope from fraying, tie wraps and duct tape were used to hold the ends of the rope together (Figure 21).This specific construction method and fasteners ensured a firm and reliable suspension of the racks, allowing the coupons to be attached and submerged in the aquatic environment in a stable and consistent manner during the study.

On September 12, 2022, three racks were installed on the platform. The racks were carefully submerged at a depth of exactly 1 meter below the surface of the water. An eye splice was applied to the ends of the rope, allowing them to be hung from iron hooks on the platforms. During the installation of the racks, sufficient distance was also kept between the sensors and the racks to prevent any influence on the sensors.

Procedure for coupon measurements

Samples were collected at two, three and six months after the start of the exposure period. Whenever samples were taken, the rack was first taken out of the water to obtain a full picture of the rack. Subsequently, four samples per rack were taken.

Three coupons were thoroughly cleaned with water, dried with paper towels, wrapped in paper towels and placed in a sealed freezer bag with silica gel to prevent further corrosion. One coupon was not cleaned and was placed in a freezer bag without touching it. The purpose of this action was to perform a visual inspection on the coupon in the future. The date and location of sampling were documented on the pouch, after which the pouch was carefully sealed. Rack was then replaced under water.

The coupons were cleaned in accordance with the guidelines set forth in the ASTM G1 standard. After cleaning, the weight loss and corrosion rate of the coupons were evaluated to understand their corrosion behaviour. Measuring the weight loss and corrosion rate provides valuable information about the interaction between the coupon material and the environment in which they are exposed and can serve as an indicator of the durability and performance of the material in corrosive conditions. To determine the corrosion rate based on the mass loss, the corrosion products were first removed from the coupons. For this purpose, the metal coupons were placed in 200 ml 23% hydrochloric acid in glass beakers for 15 minutes. After the acid treatment, the coupons were thoroughly rinsed with demineralized water and dried with paper. To ensure the accuracy of the measurement, it was ensured that the coupons were completely dry before being weighed. At the start and after the cleaning process, the coupons were photographed with the corresponding tags.

At the start of the exposure, 30 coupons, per steel grade, were used to determine the average initial masses. Subsequently, at different times (approximately 2, 3 and 6 months after exposure to seawater), four coupons were collected from each steel grade, three of which were for mass loss measurements. For the determination of the corrosion rate, the mass change of the coupons was measured and extrapolated to a corrosion rate.

Use of the CCube LP sensor

For the SOCORRO project, bespoke sensor systems been developed for corrosion measurement CCube (Delft, the Netherlands). The sensor is based on linear polarization (LP) theory to measure the rate of corrosion. This is achieved by applying small voltages (less than ±30 mV) to the metal just above and below the corrosion potential. Within this voltage range, the resulting current response is linear if the anodic and cathodic regions are equal (Campos-Silva & Rodríguez-Castro, 2015; Ropital, 2011). This makes it possible to determine the polarization resistance (Rp), which is defined as the slope of the current-potential curve according to the Stern-Geary equation (Stern & Geaby, 1957):

$$I_{Corr} = \frac{1}{R_p} * \frac{\beta_a * \beta_c}{2.303(\beta_a * \beta_c)}$$

with

$$B = \frac{\beta_a * \beta_c}{2.303(\beta_a * \beta_c)}$$

B is a constant that depends on the anodic and cathodic table diagram (β_a and β_c) obtained from polarization curves. In most cases, the values of β are between 60 and 120 mV (García-Galvan, Fajardo, Barranco, & Feliu, 2021).

$$I_{Corr} = \frac{B}{R_p}$$

Faraday's law can then be applied to calculate the corrosion rate as follows:

$$CR = K_1 * \frac{I_{Corr}}{dA} * EW$$

whereby CR = corrosion rate in mm/year, K_1 = constant of $3.27*10^{-3}$, d = density in g/cm³, EW = the equivalent weight, defined as the mass in grams oxidized by the passage of an electrical charge of 1 Faraday. EW values can be found for different metals in ASTM G102 (García-Galvan et al., 2021).

The CCube uses working electrodes made from the three different steel grades in the project (S355, 316L and S235) and a micro-electrochemical cell that measures the rate of corrosion. These measurements are performed every four hours. The working and reference electrodes are housed in a plastic housing filled with epoxy adhesive for protection against sea water, with dimensions of 150 mm (length) x 60 mm (height) x 50 mm (width).

The sensor is connected to a separate CCube control box located in an easily accessible position. A potentiostat and a data logger are installed in the control cabinet. In addition, the control box contains a mobile antenna that transmits the measured data to the CCube network. The company collects all sensor data and sends it to an online database that is accessible to all researchers of the SOCORRO project.

On 3 August 2022, the CCube probes were installed in the water for the first time, together with the environmental sensors. Due to cabling errors at the company, which only became clear after several months, all data generated by the CCube LP probe until March 1, 2023, were unusable. Afterwards, the cabling in the probes was correctly reconnected, so that the sensors have been functioning properly. However, when interpreting the CCube data, it must be considered that the sensors were not new when placed in the water and already showed some traces of corrosion. Some sensors showed more corrosion than others.

Corrosion: results

Corrosion rates obtained through coupon measurements

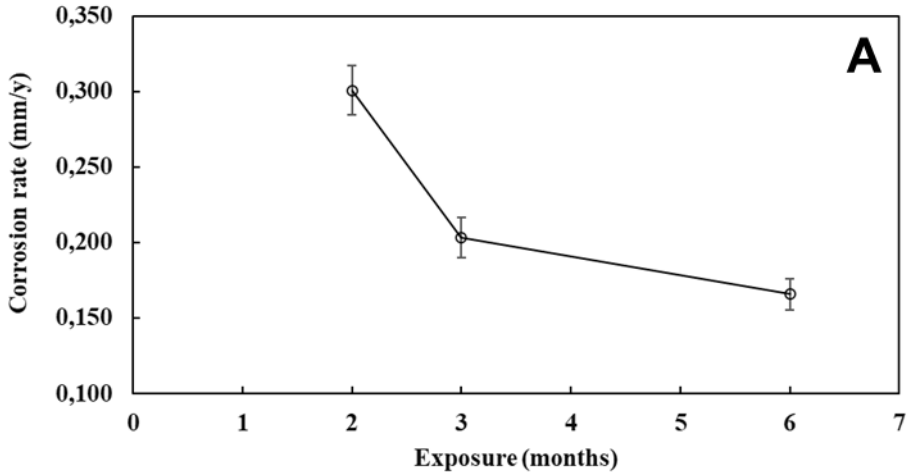

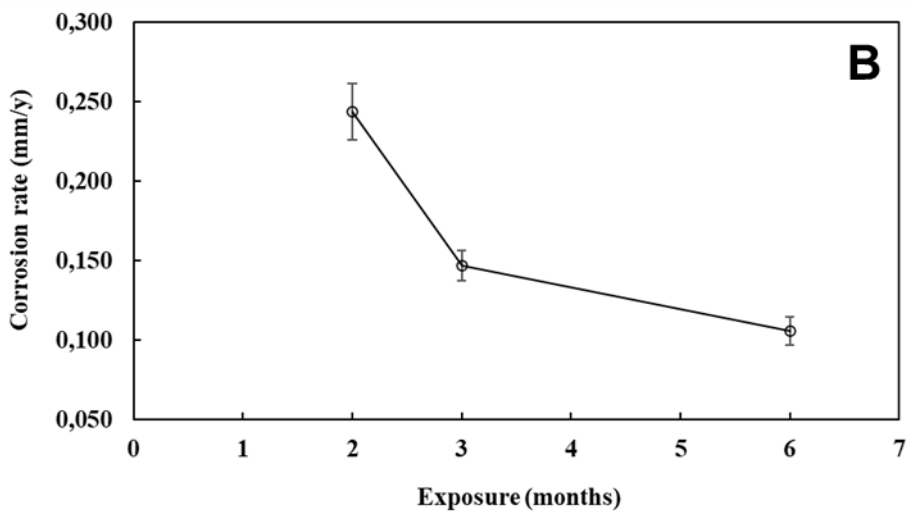

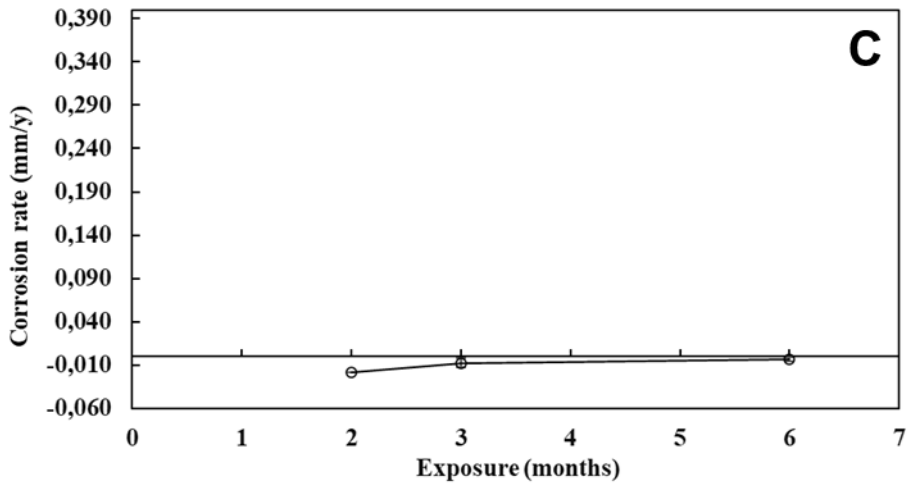

Figure 22. Corrosion rates of (A) S355, (B) S235 and (C) 316L steel coupons at the Ostend platform

Corrosion rates obtained through LP measurements

The data presented below cover the period from April 25, 2023, to May 24, 2023. The main purpose of this chapter is to investigate the reliability of the CCube sensor, which uses the LP technology. This is done by evaluating the extent to which the CCube data agrees with the data from the mass loss measurements on the sample coupons. In addition, the corrosion data from the CCube is used together with the data from the environmental sensors for a correlation analysis. It should be noted that the sensor part of the LPR measurement system in Ostend remained submerged while the corrections were made. The corrosion layers were therefore representative of a system that had been in use since the beginning of August 2023. As a result, a continuation of the corrosion curve, set up with the coupons can be expected.

The mass loss measurements for **S355** (Figure 22) indicate that the corrosion rate in Ostend has decreased to 0.166 mm/year after 6 months, and it is expected that the corrosion rate will decrease further and stabilize. However, the LPR measurements (Figure 23) show a corrosion rate between 0.300 mm/year and 0.550 mm/year, which is unlikely to be correct. Coupon data show a corrosion rate of (0.166 ± 0.006) mm/year.

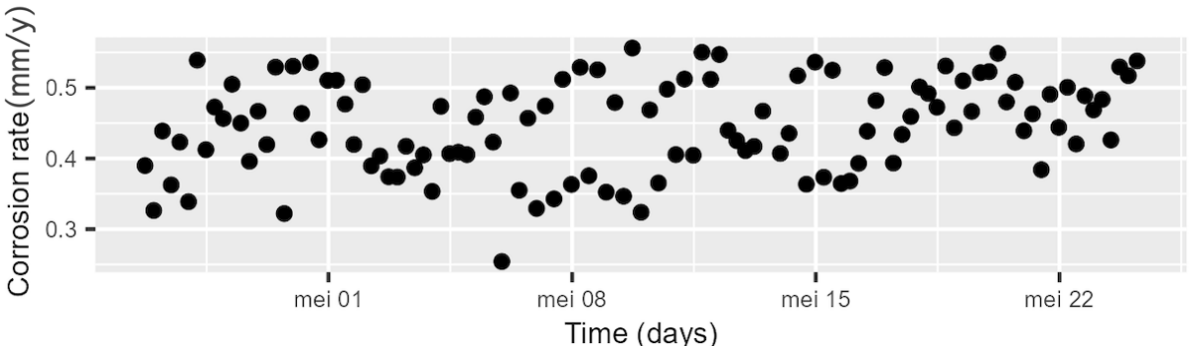

Figure 23. LPR corrosion rate measurements for S355 low carbon steel at the Ostend demonstration

The data for S235 (Figure 24) show a much lower spread than the data for S355. The CCube shows a corrosion rate between 0.080 and 0.120 mm/year This is the only setup where the CCube results are consistent with the mass loss measurements on the sample coupons where a corrosion rate of 0.106 mm/year was measured.

Figure 24. LPR corrosion rate measurements for S235 low carbon steel at the Ostend demonstration

The CCube sensors show that the corrosion rate of 316L steel is practically zero for this study. For reference, the highest measured corrosion rate for 316L by the CCube is 0.015 mm/year.

This is even lower than the corrosion rate measured with the mass loss measurement, where the initial measurement resulted in 0.034 mm/year.

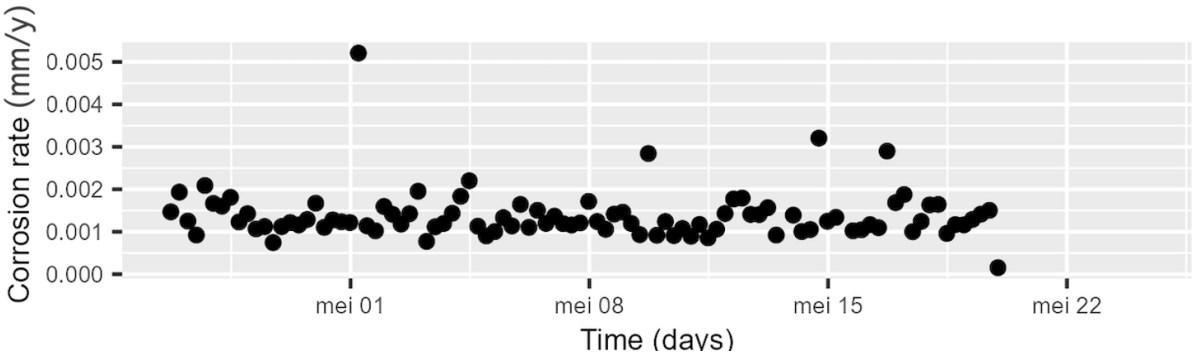

Figure 25. LPR corrosion rate measurements for 316L low carbon steel at the Ostend demonstration

Use of the SOCORRO approach

In order to test the SOCORRO algorithm, environmental parameters sere uploaded in the SOCORRO app (https://app-c14g.onrender.com/) and the outcome (corrosion rate in mm/year) was compared with the corrosion rate of the coupons (initial value).

The predicted corrosion rate for S235 steel, based on the environmental parameters is given in

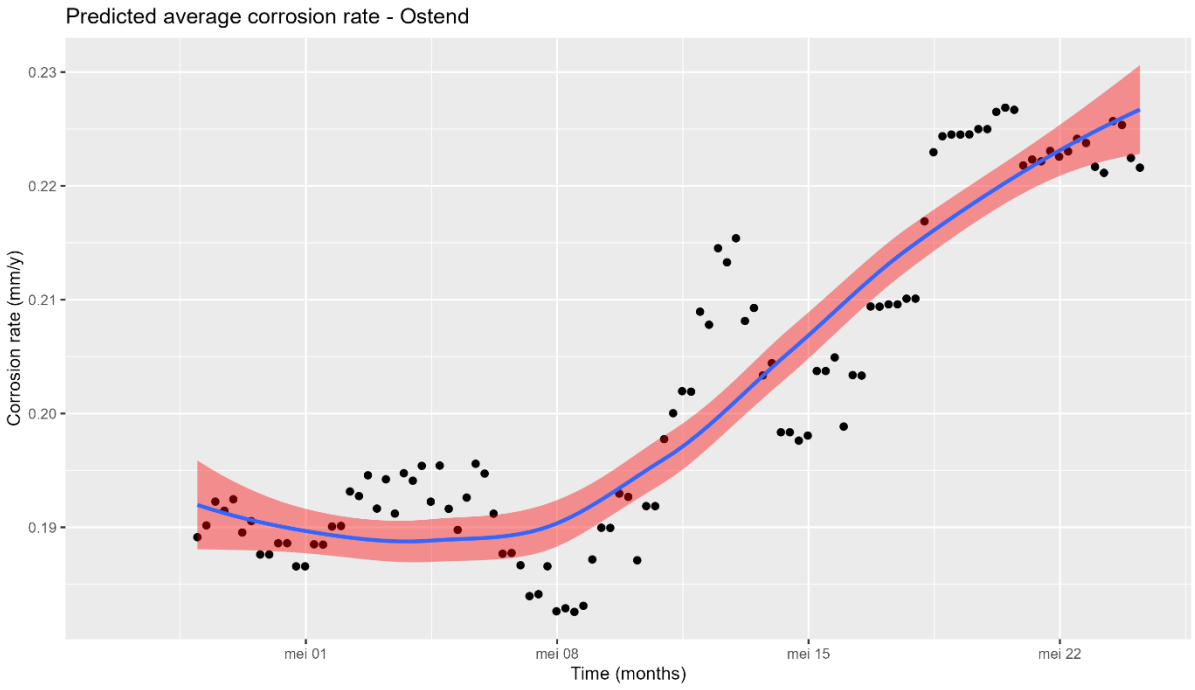

Figure 26. This predicted value fluctuates heavily in the first period (corresponding to August 2023) and slows to a value of 0.22-0.24 in the course of September to October, and to around 0.20 mm/year from November onwards. If we compare these values with the coupon

corrosion rates for the first 6 months of the experiment and with the LP data for the data measured in May 2023, we see a good correlation between LP and coupon measurements, but only for the S235 steel data.

The initial corrosion rate (measured for the first two months of the experiment) fits very well with the predicted rate by the SOCORRO algorithm. As time goes by, the predicted corrosion rate changes along with (mostly) temperature, but moves away from the physical corrosion data from both coupons and LP measurements. This suggests that there is a time factor which is still not correctly captured by the model, and which, in practice, is related to the formation of a corrosion product layer on top of the coupons as well as the LP sensors. This time-dependent decrease should be incorporated into the next versions of the algorithm.

Table 2. Comparison of corrosion rates for coupons, LP measurements and the SOCORRO algorithm. Corrosion rates are expressed in mm/year. Standard error given for coupon data (n = 3)

	2 months	3 months	6 months	8 months
Coupons	0.24 ± 0.03	0.147 ± 0.013	0.106 ± 0.012	
CCube				0.1
Algorithm	0.225	0.21	0.2	0.19-0.225

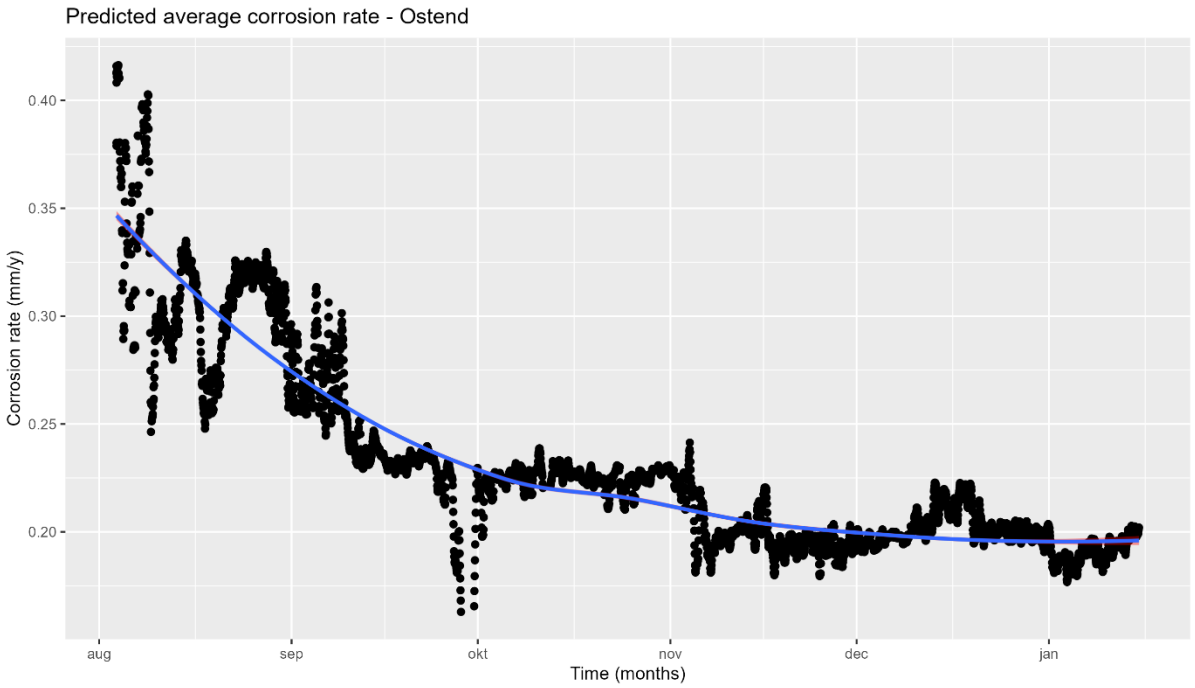

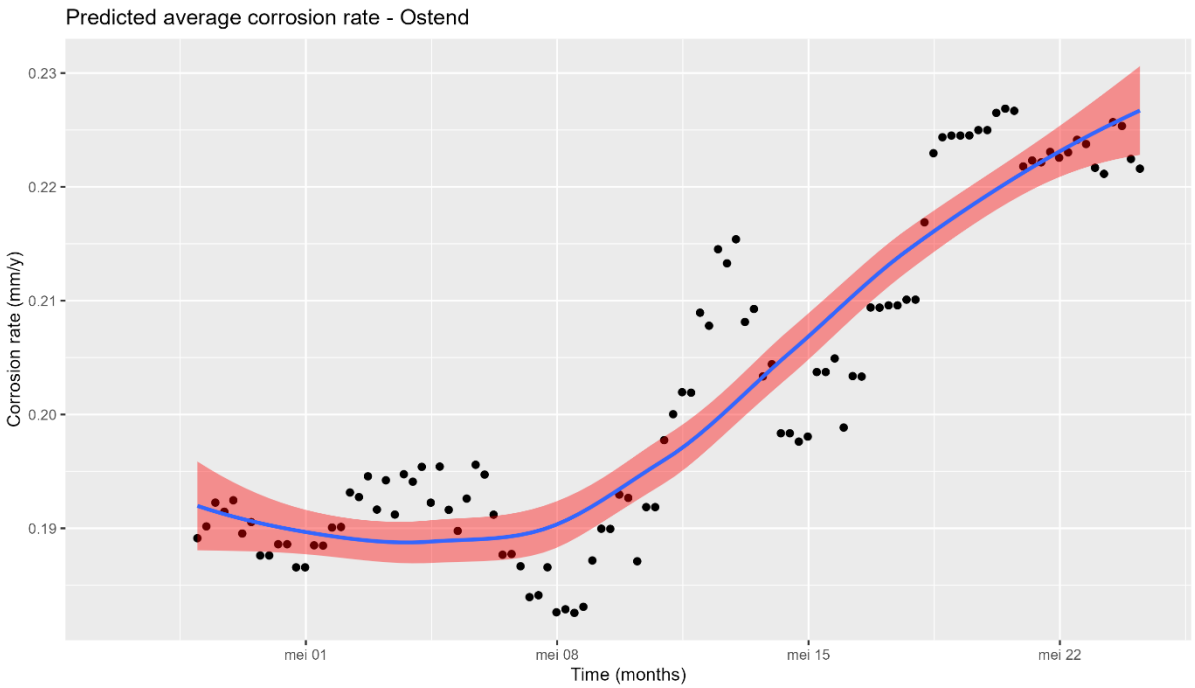

Figure 26. Predicted corrosion rate for S235 by the SOCORRO algorithm.
Top: predicted corrosion data for every time point based on local averages of the different environmental points between August 2022 and February 2023
Bottom: predicted corrosion rates for every time point based on local averages of the different environmental points in May 2023
Blue line gives a loess regression line for the dataset with a red 95% confidentiality zone.

Correlation between LPR corrosion measurements and environmental parameters

To understand how the corrosion data can be explained, we conducted a correlation analysis between the LP data and the measurements obtained from the different sensors of the Scuba 90 (Figure 27)

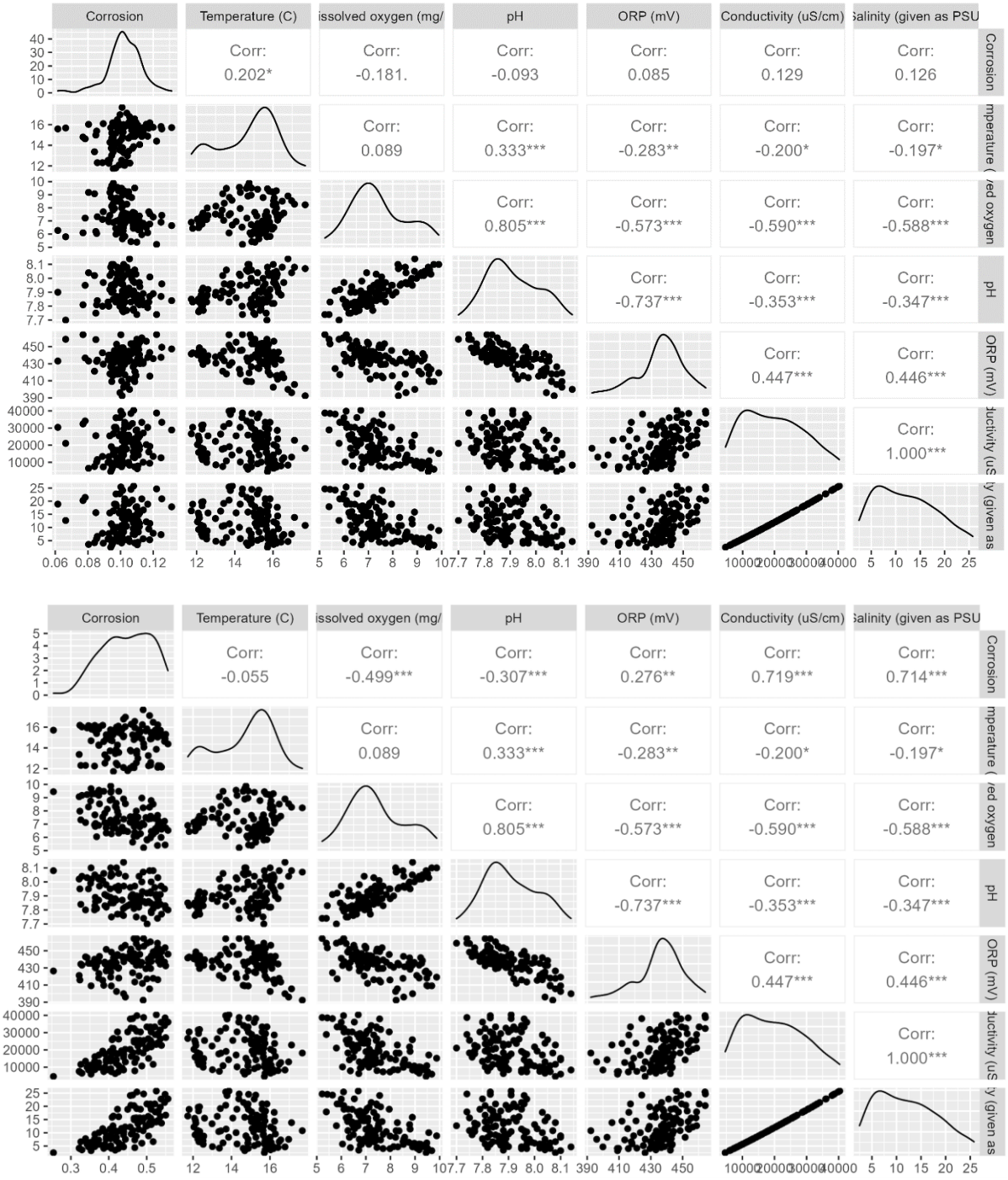

Figure 27. Correlation between corrosion rate of S235 (top) and S355 (bottom) carbon steel and the different environmental parameters as measured with the Scuba 90 Eijkelkamp probe.

The pairs plot of the correlation between the environmental parameters and the corrosion rate salinity (or specific conductivity) only shows a clear positive linear relationship between corrosion and conductivity/salinity (R-value 0.719, resp. 0.714), but onluy for the S355 steel in Ostend. This finding is not confirmed by the correlation analyzes of the other steel grades in Ostend.

Technical remarks

The CCube with LPR sensors proved to be largely impractical, as evidenced by the average corrosion rate of approximately 0.700 mm/year measured for S355 in VL1 from late April to late May, whereas mass loss measurements on March 1st indicated a corrosion rate of approximately 0.210 mm/year for S355 in VL1. This discrepancy suggests a substantial error factor of 3.

Plans for further use of the output?

The Ostend platform will continue to serve as a Living lab, managed by Antwerp Maritime Academy, as a follow-up for Interreg 2 Seas SOCORRO and Interreg Vlaanderen-Nederland Praktijklab Corrosie en Isolatie. The data obtained in this Living lab will continue to serve as a baseline for other industrial tests. For example, a comparison will be set up to compare different corrosion protection mechanisms.

The data collected will be fed into the algorithm to create a better model for marine installations, and to work out the incorporation of a time-delay effect.